MIRO1 controls energy production and proliferation of smooth muscle cells

Lan Qian, MBBS [1], Olha M. Koval, Ph.D. [1], Benney T. Endoni [1,2], Denise Juhr, B.S. [1], Colleen S. Stein, Ph.D. [1], Chantal Allamargot Ph.D.[3], Li-Hsien Lin, Ph.D.[1], Deng-Fu Guo, Ph.D.[4], Kamal Rahmouni, Ph.D.[1,2,4,6], Ryan L. Boudreau Ph.D.[1], Jennifer Streeter, M.D., Ph.D. [1], William H. Thiel, Ph.D.[1], Isabella M. Grumbach M.D., Ph.D. [1,5,6]*

Short title: MIRO1 in smooth muscle proliferation

Affiliations:
[1] Abboud Cardiovascular Research Center, Division of Cardiovascular Medicine, Department of Internal Medicine, Carver College of Medicine, University of Iowa, Iowa City IA 52242, USA.

[2] Interdisciplinary Program in Molecular Medicine, University of Iowa,

[3] Central Microscopy Research Facility, University of Iowa,

[4] Department of Neuroscience and Pharmacology, University of Iowa,

[5] Free Radical and Radiation Biology Program, Department of Radiation Oncology, Holden Comprehensive Cancer Center, University of Iowa, Iowa City IA 52242, USA.

[6] Veterans Affairs Healthcare System, Iowa City, IA 52246, USA.

*To whom correspondence should be addressed:
Isabella Grumbach, MD, PhD
University of Iowa
Dept. of Internal Medicine
169 Newton Road
Iowa City, IA 52246
isabella-grumbach@uiowa.edu

The authors have declared that no conflict of interest exists.

ABSTRACT (300 words)

Background: The outer mitochondrial Rho GTPase 1, MIRO1, mediates mitochondrial motility within cells, but implications for vascular smooth muscle cell (VSMC) physiology and its roles invascular diseases, such as neointima formation following vascular injury are widely unknown.

Methods: An in vivo model of selective Miro1 deletion in VSMCs was generated, and the animals were subjected to carotid artery ligation. The molecular mechanisms relevant to VSMC proliferation were then explored in explanted VSMCs by imaging mitochondrial positioning and cristae structure and assessing the effects on ATP production, metabolic function and interactions with components of the electron transport chain (ETC).

Results: MIRO1 was robustly expressed in VSMCs within human atherosclerotic plaques and promoted VSMC proliferation and neointima formation in mice by blocking cell-cycle progression at G1/S, mitochondrial positioning, and PDGF-induced ATP production and respiration; overexpression of a MIRO1 mutant lacking the EF hands that are required for mitochondrial mobility did not fully rescue these effects. At the ultrastructural level, Miro1 deletion distorted the mitochondrial cristae and reduced the formation of super complexes and the activity of ETC complex I.

Conclusions: Mitochondrial motility is essential for VSMC proliferation and relies on MIRO1. The EF-hands of MIRO1 regulate the intracellular positioning of mitochondria. Additionally, the absence of MIRO1 leads to distorted mitochondrial cristae and reduced ATP generation. Our findings demonstrate that motility is linked to mitochondrial ATP production. We elucidated two unrecognized mechanisms through which MIRO1 influences cell proliferation by modulating mitochondria: first, by managing mitochondrial placement via Ca^{2+}-dependent EF hands, and second, by affecting cristae structure and ATP synthesis.

Keywords: Mitochondria, MIRO1, proliferation, electron transport chain, smooth muscle, neointima

INTRODUCTION

Although mitochondria have been extensively studied in other parts of the cardiovascular system [1,2], little is known about their roles in the vascular smooth muscle cells (VSMCs) of systemic arteries, particularly with respect to vasoproliferative diseases such as neointimal hyperplasia. Initial insight was gained by extending concepts established in earlier studies of cytosolic pathways. Specifically, neointima formation was inhibited in vivo by either the promotion of apoptosis via mitochondrial pathways [3-5] or by reducing mitochondrial ROS production through the overexpression of uncoupling protein 2 or superoxide dismutase 2 [6-8]. Mitochondrial fission/fusion is recognized as a regulator of VSMC proliferation, migration, and neointima formation. Fission/fusion of mitochondria is regulated by the mitochondrial membrane proteins dynamin-related proteins and mitofusin proteins [9-11]. Moreover, over a decade ago, Chalmers and colleagues demonstrated that mitochondria in proliferating VSMCs are mobile and that interference with their mobility blocks proliferation [12]. However, the molecular regulators were not further investigated.

The outer mitochondrial membrane GTPase MIRO1 is essential for orchestrating mitochondrial positioning in many cell types, including neurons, lymphocytes, and various cancer cell lines [13-16]. The MIRO1 protein contains two canonical EF-hand domains that are flanked by two GTPase domains and a C-terminal transmembrane domain that anchors MIRO1 to the outer mitochondrial membrane [17]. MIRO1 associates with trafficking kinesin-binding proteins (TRAKs), linking mitochondria to microtubules and myosin XIX [13-15,18]. These interactions are regulated by changes in intracellular Ca^{2+} levels: when MIRO1 is not bound by Ca^{2+}/calmodulin, it links mitochondria to microtubules; when the EF hands are bound by Ca^{2+}, a conformational change causes mitochondria to dissociate from microtubules, arresting their movement [13]. In addition to playing a role in promoting mitochondrial mobility, MIRO1 is believed to control mitophagy through phosphorylation by the Pink/Parkin complex [19,20], and to facilitate the formation of

mitochondrial cristae via associations with the mitochondrial contact site (MICOS) complex and the mitochondrial intermembrane space bridging (MIB) complex [21].

The reports that MIRO1 regulates mitochondrial dynamics, mitophagy, cell survival and apoptosis, and controls inter-organelle communication have prompted some investigations into its role in human diseases. For example, Miro1 mutations identified in humans (for example p.R272Q) have been linked genetically and pathophysiologically to Parkinson's disease [19,20,22]. Nevertheless, few studies have investigated its impact on cardiovascular disease. In vitro studies of cardiomyocytes isolated from neonatal rats lacking Miro1 revealed that this deficiency protects against phenylephrine-induced cardiomyocyte hypertrophy and mitochondrial fission [23]. The extent to which MIRO1 deficiency contributes to vascular disease remains largely unstudied, with the exception of our laboratory's demonstration that Miro1 deletion impairs VSMC migration in vitro [24].

The goal of this study was to determine whether MIRO1 controls VSMC proliferation and, if so, to uncover the underlying mechanisms involved. We investigated the effects of MIRO1 manipulation on VSMC proliferation and the potential mechanism by which MIRO1 affects cell cycle progression, mitochondrial mobility, ATP production, and respiration. Additionally, we used a transgenic mouse model in which Miro1 was deleted specifically in VSMCs to test its effects on neointima formation in vivo.

METHODS

Data Availability

In accordance with the Transparency and Openness Promotion Guidelines, the authors declare that all supporting data and Supplemental Material are available from the corresponding authors upon reasonable request. The Supplemental Methods and the Major Resource Table can be found in the Supplemental Material.

Animals

Animal studies were conducted in accordance with the NIH *Guide for the Care and Use of Laboratory Animals*, following protocols that were approved by the Institutional Animal Care and Use Committee (IACUC) of the University of Iowa. SMMHC-CreER^{T2} mice, in which expression of tamoxifen-inducible Cre recombinase is driven by the smooth muscle myosin heavy chain (SMMHC) promoter, were obtained from The Jackson Laboratory. The Mitochondrial Rho1 GTPase LoxP (Floxed Miro1 conditional KO) mice were graciously provided by Dr. Janet Shaw (University of Utah). The VSMC-selective floxed Miro1 conditional knockout mice (SM-Miro1$^{-/-}$ mice) were generated by crossbreeding with SMMHC-CreER^{T2} mice. Cre recombination was induced by intraperitoneal injection of tamoxifen (80 mg/Kg) for 5 days, followed by a 14-day break. SMMHC-CreER^{T2} mice were injected with same dose of tamoxifen and used as a control for in vivo experiments. In vivo experiments were performed in male mice because the tamoxifen inducible Cre recombinase in this model, whose expression is driven by the SMMHC promoter, is present on the Y-chromosome.

Ligation of the common carotid artery and preparation of vessels for quantification of neointima and media

10–12-week-old SM-Miro1$^{-/-}$ mice and SMMHC-CreER^{T2} controls were fed a high-fat diet for 3 weeks and then the animals were anesthetized, and survival surgeries of left common carotid

artery ligation were performed. At 21 days after the surgery, the animals were anesthetized and underwent transcardiac perfusion with 10 ml of PBS, followed by fixation with 10 ml of 4% paraformaldehyde (PFA), at physiological pressure. The left (ligated) and right (non-ligated) common carotid arteries were excised at the carotid bifurcation and embedded for sectioning followed by Verhoeff Van Gieson (VVG) staining.

Culture of vascular smooth muscle cells (VSMCs)

Primary mouse aortic VSMCs were isolated enzymatically; incubation in elastase (1U/ml for 10 min at 37º) was performed to remove the adventitia. The medial layer of the aorta, which contains the VSMCs, was minced and incubated in 2 mg/ml collagenase type II digestion solution (Worthington Biochemical Corporation) for 2 hr. In early experiments, VSMCs were isolated from SM-Miro1$^{-/-}$ and littermate mice (referred to as SM-Miro1$^{-/-}$ VSMCs). In later experiments, VSMCs were isolated from Miro1$^{fl/fl}$ mice and had been transduced with adenoviruses expressing Cre recombinase at a multiplicity of infection (MOI) of 50 for 2 weeks (referred to as MIRO1$^{-/-}$ VSMCs). VSMCs from littermate controls were subjected to the same procedure with empty adenovirus.

Statistical Analysis

The sample size (n) and the statistical tests used are indicated in each figure legend.

RESULTS

Loss of MIRO1 blocks neointima formation.

To study the effects of MIRO1 on smooth muscle cell biology after vascular injury, we generated a transgenic model in which MIRO1 is selectively deleted in smooth muscle cells after administration of tamoxifen (SM-MIRO1$^{-/-}$, figure S1A). Reduced levels of MIRO1 mRNA and protein in carotid arteries and the aorta were confirmed by immunohistochemistry, western blotting, and quantitative real time PCR (figure 1A, figure S1A, B). Mice of both the wild type and SM-MIRO1$^{-/-}$ genotypes were fed a high-fat diet for three weeks, and then vascular injury was induced by ligation of the common carotid artery. Three weeks after ligation, the mice were euthanized and neointima size was assessed. Neointima formation was robust in wild type mice and significantly reduced in SM-MIRO1$^{-/-}$ mice (figure 1B). The neointimal and medial areas were smaller in the arteries from the SM-MIRO1$^{-/-}$ mice than in those of their wild type counterparts (figure 1C, D), and the same was true for both the neointimal area 250 μm from the ligation site and the cumulative neointimal area over the first one mm of the carotid artery proximal to the ligation (figure 1E, F). Immunohistochemical analysis of tissue from ligated mouse arteries revealed that MIRO1 was robustly expressed in VSMCs of the neointima (figure 1G). Lastly, we confirmed that MIRO1 is present in the coronary artery of a human subject with atherosclerotic disease. Notably, in both the aortic media and the atherosclerotic plaque of this subject, MIRO1 was expressed in cells positive for smooth-muscle actin (figure 1G, H).

Loss of MIRO1 reduces the proliferation of smooth muscle cells.

To determine the relevance of MIRO1 to cell proliferation, VSMCs were explanted from the aortas of SM-MIRO1$^{-/-}$ mice and cultured. Platelet-derived growth factor (PDGF) was used to enhance cell proliferation. The cell number was assessed 3 days after plating (figure S2A). In the case of wild type cells, the number was approximately 80% greater for those treated with PDGF than for those not treated with PDGF. In the case of SM-MIRO1$^{-/-}$ VSMCs, cell counts

were lower in both the PDGF-treated and non-treated cells, particularly in the former (figure S2A).

Given the generally poor proliferation of VSMCs from SM-MIRO1$^{-/-}$ mice, in later experiments we used VSMCs isolated from MIRO1$^{fl/fl}$ mice and infected them with adenovirus expressing cre (Ad Cre; these cells are henceforth denoted as Miro1$^{-/-}$). As negative controls, we used cells isolated from the same mice infected with an empty vector control adenovirus (Ad EV). In this model, cre recombination was efficient (figure 2A). At 72 hr after plating in growth medium, the number of Miro1$^{-/-}$ VSMCs was significantly lower than that of wild type cells, both when the cells were grown under the same conditions and when they were additionally treated with PDGF (figure 2B). Cells were synchronized by serum starvation for 48 hr and FACS analysis was performed to identify the phase of the cell cycle during which the growth delay caused by a lack of MIRO1 occurred (figure 2C-F). At baseline (0 hr), no differences in the cell cycle distribution were observed across the experimental groups (figure 2D). At 24 hr, however, significantly more wild type than MIRO$^{-/-}$ VSMCs had exited the G1 phase. At 48 hr, most wild type VSMCs had returned to a baseline-like cell cycle distribution, suggesting that the cell cycle was completed, whereas more MIRO1$^{-/-}$ VSMCs remained in S phase and fewer were in G1 phase (figure 2D-F).

Immunoblotting for cyclin D1 and cyclin E revealed significant decreases in the G1 phase and in the G1/S transition in MIRO1$^{-/-}$ VSMCs (figure 3A-C), consistent with the results of the FACS analysis. Subsequent progression through later cell cycle phases was also affected. In the VSMCs that had been arrested in G1/S phase by exposure to aphidicolin and then treated with growth media for 24 hr, the levels of cyclin A and B, as well as the phosphorylation of histone H3, were significantly lower in the MIRO1$^{-/-}$ VSMCs, (figure 3D-H). We also tested the extent to which the reconstitution of MIRO1 in MIRO1$^{-/-}$ VSMCs rescued cell proliferation. Expressing wildtype MIRO1 at levels similar to those in wild type cells normalized proliferation, whereas expressing a MIRO1 mutant lacking the EF hands at same levels only partially rescued cell

proliferation (figure 3I, J). These data demonstrate that MIRO1 is required for cell proliferation, that it affects cell cycle progression early (during G1/S-phase), and that the EF hands of MIRO1 are necessary for normal cell proliferation.

Loss of MIRO1 impairs mitochondrial mobility in proliferating VMSCs.

The EF hands of MIRO1 mediate the attachment to microtubules in neurons and without them, mitochondria do not move normally within axons [13]. To determine the extent to which MIRO1 contributes to mitochondrial mobility in VSMCs, we plated wild type or MIRO1$^{-/-}$ VSMCs on microchips (CYTOOchip^{TM}) with Y-patterns. In wild type VSMCs, after cell-cycle arrest caused by serum starvation, the mitochondria were concentrated around the nucleus. At 6 hr after treatment in growth media supplemented with PDGF, the mitochondria were distributed throughout the cell, including near the cell edges (figure 4A-C). In the MIRO1$^{-/-}$ VSMCs, however, the mitochondria remained near the nucleus. Reconstitution of MIRO1$^{-/-}$ VSMCs with wild type MIRO1 fully rescued the mitochondrial distribution at 6 hr after PDGF treatment (Figure 4D-G). In contrast, after transduction of MIRO1$^{-/-}$ VSMCs with the MIRO1 mutant KK (MIRO1-KK), which lacks functional EF hands, the mitochondria were irregularly and unequally distributed (Figure 4D-G).

We then determined whether mitochondrial ATP production is necessary for mitochondrial mobility or VSMC proliferation. For this purpose, we added oligomycin, an inhibitor of ATP synthesis, to proliferating wild type VSMCs for 72 hr. This treatment reduced the number of VSMCs (figure 5A) as well as in the intracellular ATP level (figure 5B). To test the effect of ATP production by mitochondria on their mobility, we assessed the mitochondrial distribution in wild type VSMCs plated on micropatterned CYTOOchips. Mitochondrial mobility was reduced when ATP production was inhibited by oligomycin (figure 5C-F). Thus far, we demonstrated that mitochondrial mobility is impaired in MIRO1$^{-/-}$ VSMCs and in wild type VSMCs with decreased

mitochondrial ATP production. To investigate whether blocking mitochondrial mobility affects ATP levels, we performed control experiments using microtubule disassembly. Nocodazole, which inhibits microtubule assembly, effectively arrested mitochondrial mobility in this assay. However, ATP levels were not affected (Figure 5F, G).

Loss of MIRO1 leads to impaired metabolic activity and reduced proliferative capacity.

Our findings that mitochondrial mobility is controlled by MIRO1 and depends on mitochondrial ATP production imply that Miro1 deletion causes a defect in metabolic activity (figure 5). Given cell proliferation is impaired at the early stages of the cell cycle in VSMCs with MIRO1 deletion and that intracellular ATP demands are high during the G1/S transition (figure 4) [25,26], we measured intracellular ATP levels in cells after 16 hr of PDGF treatment (figure 6A, B). ATP levels were significantly lower in MIRO1$^{-/-}$ VSMCs than in their wild type counterparts. Additionally, transduction with MIRO1-WT normalized ATP production, whereas transduction with MIRO1-KK did not (figure 6C). AMP kinase is an intracellular indicator of the metabolic state and regulates the expression of cyclins D and E. Thus, we determined AMP kinase activation by immunoblotting. In MIRO1$^{-/-}$ VSMCs, the phosphorylation of AMP kinase was elevated, indicating an intracellular energy deficiency (figure 6D-F). Moreover, the expression of p53 and p21 increased and cyclin D1 expression decreased (figure 6G-I), supporting a link between energy levels and cell-cycle progression in the G1/S phase. We also measured the oxygen consumption rate in wildtype and Miro1$^{-/-}$ VSMCs by Seahorse. We detected decreased basal respiration in MIRO1$^{-/-}$ VSMCs treated with PDGF compared to wild type (figure 6J, K). However, the rate of extracellular acidification, a measure of glycolysis, was not significantly affected in MIRO1$^{-/-}$ VSMCs (figure 6L), indicating a lack of compensatory upregulation of glycolysis.

MIRO1 controls electron transport chain (ETC) activity

We sought to establish the mechanism by which MIRO1 controls ATP production. Previous findings in embryonic fibroblasts have suggested that MIRO1 associates with both the mitochondrial contact site (MICOS) complex and the mitochondrial intermembrane space bridging (MIB) complex, which collectively control the folding of mitochondrial cristae [21]. We assessed the effect of MIRO1 deletion on the formation of mitochondrial cristae in VSMCs by transmission electron microscopy. Consistent with findings in fibroblasts [21], we found that in Miro1$^{-/-}$ VSMCs, the cristae were less dense than those in wild type controls, and their morphology was distorted (figure 7A-C). Next, we established the associations of wild type MIRO1, MIRO1-KK, and a MIRO1 mutant lacking the C-terminal transmembrane domain with components of the electron transport chain and the MIB/MICOS complex. Pull-down experiments in HEK 293T cells revealed interactions between MIRO1 and several MIB/MICOS proteins (Sam50, Mic60, and Mic19; figure 7D-G) and NDUFA9 subunits of electron transport chain complex I (figure 7H). The transmembrane domain by which MIRO1 is attached to mitochondria was necessary for the association with all proteins, and in the absence of the EF hands the association with all proteins was weaker. The expression of proteins of the MIB/MICOS complex was not affected by MIRO1 deletion (figure S3).

In the case of the ETC complexes, immunoblotting for subunits of all five electron transport chain complexes was evaluated, but this did not reveal a significant difference in protein levels between wild type and MIRO1$^{-/-}$ VSMCs (figure S3). Because the formation of mitochondrial cristae affects the formation of the MIB/MICOS super complex and the activity of the ETC chain, we tested the abundance of mitochondrial super complexes in blue native gels (figure 7I, J). The levels of super complex II were lower in MIRO1$^{-/-}$ VSMCs then in wild type VSMCs (figure 7J). We also tested the activity of ETC complex I by measuring the consumption of NADH. In MIRO1$^{-/-}$ cells, the activity of this complex was significantly decreased (figure 7K, L). These data

demonstrate that MIRO1 associates with MIB/MICOS and that this interaction promotes the formation of mitochondrial super complexes and the activity of ETC complex I.

Pharmacological reduction of MIRO1 impairs VSMC proliferation

Finally, we tested whether the pharmacological reduction in MIRO1 yields effects on cell proliferation and ATP production similar to those observed with the genetic deletion of the protein. Recently, a small-molecule MIRO1 reducer [20] was developed that removes MIRO1 specifically from mitochondria, leading to the loss of mitochondria through increased mitophagy. In wild type VSMCs, incubation with this compound for 72 hr reduced mitochondrial mass (figure S4A, B). It also decreased the number of proliferating VSMCs at 72 hr (figure S4C). The effect of the reducer on cell number was dose-dependent (figure S4D). Furthermore, the compound also lowered intracellular ATP levels in wild type VSMCs (figure S4E). These findings suggest that reducing MIRO1 could be utilized to treat vasoproliferative diseases, such as neointima formation.

DISCUSSION

In this study, we established that the outer mitochondrial membrane GTPase MIRO1 is essential for VSMC proliferation and neointima formation. Our findings provide significant insights into the mechanisms by which MIRO1, ATP production, and mitochondrial mobility regulate cell proliferation.

Firstly, we discovered that neointima formation is abolished in a mouse model with VSMC-specific MIRO1 deletion, and that cell proliferation in cultured aortic VSMCs lacking MIRO1 is significantly reduced due to delays in the early phases of the cell cycle. Unlike previous research primarily focusing on the role of MIRO1 in neurons and embryonic fibroblasts [16,19-21,27-31], our findings extend its importance to primary proliferating vascular smooth muscle cells, revealing its critical involvement in VSMC proliferation and neointima formation. We are the first to demonstrate that MIRO1 deletion in VSMCs results in abolished neointima formation in a mouse model, highlighting MIRO1 as a potential new therapeutic target for treating vasoproliferative diseases.

In immortalized cells lacking MIRO1 and 2[16], impaired cytokinesis with asymmetric partitioning of mitochondria to daughter cells was reported in M-phase [32]. Although we detected reduced progression in the G2/M phase in MIRO1$^{-/-}$ VSMCs, we also found strong evidence for impairments in the early phases of the cell cycle.

Secondly, the loss of MIRO1 led to reduced intracellular ATP levels and abolished mitochondrial mobility. This indicates that MIRO1 is crucial for maintaining both energy production and the dynamic distribution of mitochondria within the cell. We also provide new evidence on the relationship that mitochondrial energy production is required for mitochondrial mobility.

VSMCs are believed to mostly rely on glycolysis to fuel their proliferation [33]. However, recent studies have provided evidence that, analogous to proliferating cancer cells, VSMCs also depend on glutaminolysis [34 35], which shuttles metabolites to the TCA cycle and promotes oxidative phosphorylation. Our findings indicate that VSMCs require ATP synthase activity since ATP synthase inhibition blocks mitochondrial mobility and VSMC proliferation. In our study, blocking mitochondrial mobility by microtubule disassembly did not decrease overall intracellular ATP levels in VSMCs. Thus, we posit that mitochondrial mobility controlled by MIRO1 enables subcellular mitochondrial positioning within VSMCs, which then supports localized subcellular ATP and ROS production. MIRO1 ensures that mitochondrial metabolites exert their effects on local targets, similar to findings in embryonic fibroblasts [36,37].

Thirdly, we found that the reconstitution of MIRO1$^{-/-}$ VSMCs with MIRO1-WT normalized cell proliferation, ATP levels, and mobility, whereas the reconstitution of MIRO1-KK, which lacks EF hands, resulted in only partial recovery. These results suggest that the EF hands of MIRO1 are important for its full functionality in VSMCs. In neurons, MIRO1 regulates the anterograde transport of mitochondria along microtubules [16,38,39]. Mitochondrial arrest in response to elevated Ca^{2+} in subcellular domains and synaptic activity is driven by the Ca^{2+}-sensing EF hands [28,40]. Here, we provide evidence that without the intracellular arrest by Ca^{2+}, VSMC proliferation is reduced. We speculate that the loss of EF hands impairs alignment and metabolite transfer at mitochondrial-ER contact sites.

Fourthly, MIRO1 loss caused an intracellular energy deficit, increased AMP kinase phosphorylation, and reduced the expression of proteins promoting the G1/S cell-cycle transition. This finding suggests a mechanism where MIRO1 influences cell proliferation through its impact on cellular energy status and cell cycle regulatory proteins. Indeed, a link between AMP kinase activation and upregulation of p53 and G1/S cell cycle arrest has been described

[25,41]. Here, our data provide an explanation for how low ATP levels caused by MIRO1 deletion block cell cycle progression at this cell cycle stage.

Fifth, we observed that MIRO1 loss impaired the formation of mitochondrial cristae as observed in embryonic fibroblasts [21]. In our model of VSMCs with MIRO1 deletion, this correlated with reduced formation of ETC supercomplexes and activity of ETC complex I. In agreement with a prior study, MIRO1 associated with MIC19, MIC60 and SAM50 and the expression of MICOS/MIB proteins were not impaired with MIRO1 deletion [21]. In addition, we detected an association between NDUFA9, a subunit of ETC complex I, and decreased ETC complex I activity. These findings provide a potential mechanism by which MIRO1 controls mitochondrial ATP production, in addition to putative decreasing metabolite transfer at distorted mitochondrial ER contact sites [16,21] .

Some findings of our study agree with published data on MIRO1, which have highlighted its role in mitochondrial dynamics, energy production, and cell signaling. Previous studies have shown that MIRO1 is involved in the regulation of mitochondrial transport and positioning, which are critical for metabolic signaling [13,15,36,42]. The observed effects of MIRO1 loss on ATP production and mitochondrial structure in our study align with reports indicating that MIRO1 dysfunction can lead to impaired mitochondrial respiration and energy deficits [15,21,36,39]. Additionally, the role of MIRO1 in cell proliferation is supported by the literature demonstrating its involvement in mitotic spindle formation at later stages of the cell cycle and [15,16,21].

Despite these compelling findings, our study has limitations. One limitation is the use of a mouse model, which, while informative, may not fully replicate human VSMC behavior. Additionally, our experiments focused primarily on cultured aortic VSMCs, which may not entirely represent the in vivo environment. Future studies should include a broader range of

VSMC models and in vivo validations to confirm these mechanisms. Moreover, MIRO1 shares 60% sequence identity with its paralog MIRO2 [27]. Both are ubiquitously expressed in eukaryotes, yet they are not functionally redundant [16,39]. In VSMCs with MIRO1 deletion, we did not detect a compensatory upregulation of MIRO2. The functions of MIRO2 in the vasculature are currently unknown. However, a previous study proposed that after trans-aortic banding, the expression of MIRO2 in cardiac myocytes improved mitochondrial function [43].

In conclusion, our study demonstrated that MIRO1 is a pivotal regulator of VSMC proliferation and neointima formation. Our study revealed the specific mechanisms by which MIRO1 regulates ATP production and mitochondrial mobility, linking these processes to cell cycle progression and energy homeostasis. This connection between mitochondrial dynamics and cell proliferation is a significant advancement in understanding how mitochondrial dysfunction can contribute to vascular disease. These findings suggest that targeting MIRO1 could be a potential therapeutic strategy for treating vasoproliferative diseases, such as neointima formation. Further research is needed to fully understand the downstream effects of MIRO1 loss and to explore the potential clinical applications of these insights.

Acknowledgements: The authors thank Dr. Christine Blaumueller of the Scientific Editing and Research Communication Core at the University of Iowa Carver College of Medicine for critical reading of the manuscript.

Sources of Funding: This project was supported by grants from the NIH (R01 HL 108932 to IMG and R01 HL 157956 to IMG and WHT); the Department of Veterans Affairs (I01 BX000163 to IMG); and the American Heart Association (17GRNT33660032 to IMG and 22PRE902649 to BTE). The contents of this article do not represent the views of the Department of Veterans Affairs or the US Government.

REFERENCES

1. Ballinger SW. Mitochondrial dysfunction in cardiovascular disease. *Free Radic Biol Med*. 2005;38:1278-1295. doi: 10.1016/j.freeradbiomed.2005.02.014
2. Wang Y, Tabas I. Emerging roles of mitochondria ROS in atherosclerotic lesions: causation or association? *J Atheroscler Thromb*. 2014;21:381-390.
3. Deuse T, Hua X, Wang D, Maegdefessel L, Heeren J, Scheja L, Bolanos JP, Rakovic A, Spin JM, Stubbendorff M, et al. Dichloroacetate prevents restenosis in preclinical animal models of vessel injury. *Nature*. 2014;509:641-644. doi: 10.1038/nature13232
4. Lv L, Meng Q, Ye M, Wang P, Xue G. STAT4 deficiency protects against neointima formation following arterial injury in mice. *J Mol Cell Cardiol*. 2014;74:284-294. doi: 10.1016/j.yjmcc.2014.06.001
5. Guo X, Chen KH, Guo Y, Liao H, Tang J, Xiao RP. Mitofusin 2 triggers vascular smooth muscle cell apoptosis via mitochondrial death pathway. *Circ Res*. 2007;101:1113-1122. doi: 10.1161/CIRCRESAHA.107.157644
6. Vendrov AE, Vendrov KC, Smith A, Yuan J, Sumida A, Robidoux J, Runge MS, Madamanchi NR. NOX4 NADPH Oxidase-Dependent Mitochondrial Oxidative Stress in Aging-Associated Cardiovascular Disease. *Antioxid Redox Signal*. 2015. doi: 10.1089/ars.2014.6221
7. Wang JN, Shi N, Chen SY. Manganese superoxide dismutase inhibits neointima formation through attenuation of migration and proliferation of vascular smooth muscle cells. *Free radical biology & medicine*. 2012;52:173-181. doi: 10.1016/j.freeradbiomed.2011.10.442 [doi]
8. Zhang Y, Li W, Wang P, Gu R, Feng Y, Wei S, Peng K, Su L, Wang Q, Li, et al. Uncoupling Protein 2 Inhibits Myointimal Hyperplasia in Preclinical Animal Models of Vascular Injury. *J Am Heart Assoc*. 2017;6. doi: 10.1161/JAHA.117.006593
9. Wang L, Yu T, Lee H, O'Brien DK, Sesaki H, Yoon Y. Decreasing mitochondrial fission diminishes vascular smooth muscle cell migration and ameliorates intimal hyperplasia. *Cardiovasc Res*. 2015;106:272-283. doi: 10.1093/cvr/cvv005
10. Lim S, Lee SY, Seo HH, Ham O, Lee C, Park JH, Lee J, Seung M, Yun I, Han SM, et al. Regulation of mitochondrial morphology by positive feedback interaction between PKCdelta and Drp1 in vascular smooth muscle cell. *J Cell Biochem*. 2015;116:648-660. doi: 10.1002/jcb.25016
11. Umezu R, Koga JI, Matoba T, Katsuki S, Wang L, Hasuzawa N, Nomura M, Tsutsui H, Egashira K. Macrophage (Drp1) Dynamin-Related Protein 1 Accelerates Intimal Thickening After Vascular Injury. *Arterioscler Thromb Vasc Biol*. 2020;40:e214-e226. doi: 10.1161/ATVBAHA.120.314383
12. Chalmers S, Saunter C, Wilson C, Coats P, Girkin JM, McCarron JG. Mitochondrial motility and vascular smooth muscle proliferation. *Arterioscler Thromb Vasc Biol*. 2012;32:3000-3011. doi: 10.1161/ATVBAHA.112.255174
13. Wang X, Schwarz TL. The mechanism of Ca2+ -dependent regulation of kinesin-mediated mitochondrial motility. *Cell*. 2009;136:163-174. doi: 10.1016/j.cell.2008.11.046
14. Morlino G, Barreiro O, Baixauli F, Robles-Valero J, Gonzalez-Granado JM, Villa-Bellosta R, Cuenca J, Sanchez-Sorzano CO, Veiga E, Martin-Cofreces NB, et al. Miro-1 links mitochondria and microtubule Dynein motors to control lymphocyte migration and polarity. *Mol Cell Biol*. 2014;34:1412-1426. doi: 10.1128/MCB.01177-13
15. Schuler MH, Lewandowska A, Caprio GD, Skillern W, Upadhyayula S, Kirchhausen T, Shaw JM, Cunniff B. Miro1-mediated mitochondrial positioning shapes intracellular energy gradients required for cell migration. *Mol Biol Cell*. 2017;28:2159-2169. doi: 10.1091/mbc.E16-10-0741

16. Lopez-Domenech G, Covill-Cooke C, Ivankovic D, Halff EF, Sheehan DF, Norkett R, Birsa N, Kittler JT. Miro proteins coordinate microtubule- and actin-dependent mitochondrial transport and distribution. *EMBO J*. 2018;37:321-336. doi: 10.15252/embj.201696380
17. Fransson S, Ruusala A, Aspenstrom P. The atypical Rho GTPases Miro-1 and Miro-2 have essential roles in mitochondrial trafficking. *Biochem Biophys Res Commun*. 2006;344:500-510. doi: 10.1016/j.bbrc.2006.03.163
18. Oeding SJ, Majstrowicz K, Hu XP, Schwarz V, Freitag A, Honnert U, Nikolaus P, Bahler M. Identification of Miro1 and Miro2 as mitochondrial receptors for myosin XIX. *J Cell Sci*. 2018;131. doi: 10.1242/jcs.219469
19. Safiulina D, Kuum M, Choubey V, Gogichaishvili N, Liiv J, Hickey MA, Cagalinec M, Mandel M, Zeb A, Liiv M, et al. Miro proteins prime mitochondria for Parkin translocation and mitophagy. *EMBO J*. 2019;38. doi: 10.15252/embj.201899384
20. Hsieh CH, Li L, Vanhauwaert R, Nguyen KT, Davis MD, Bu G, Wszolek ZK, Wang X. Miro1 Marks Parkinson's Disease Subset and Miro1 Reducer Rescues Neuron Loss in Parkinson's Models. *Cell Metab*. 2019;30:1131-1140 e1137. doi: 10.1016/j.cmet.2019.08.023
21. Modi S, Lopez-Domenech G, Halff EF, Covill-Cooke C, Ivankovic D, Melandri D, Arancibia-Carcamo IL, Burden JJ, Lowe AR, Kittler JT. Miro clusters regulate ER-mitochondria contact sites and link cristae organization to the mitochondrial transport machinery. *Nat Commun*. 2019;10:4399. doi: 10.1038/s41467-019-12382-4
22. Chemla A, Arena G, Onal G, Walter J, Berenguer-Escuder C, Grossmann D, Grünewald A, Schwamborn JC, Krüger R. Generation of two induced pluripotent stem cell lines and the corresponding isogenic controls from Parkinson's disease patients carrying the heterozygous mutations c.815G > A (p.R272Q) or c.1348C > T (p.R450C) in the RHOT1 gene encoding Miro1. *Stem Cell Res*. 2023;71:103145. doi: 10.1016/j.scr.2023.103145
23. Conejeros C, Parra V, Sanchez G, Pedrozo Z, Olmedo I. Miro1 as a novel regulator of hypertrophy in neonatal rat cardiomyocytes. *J Mol Cell Cardiol*. 2020;141:65-69. doi: 10.1016/j.yjmcc.2020.03.014
24. Koval OM, Nguyen EK, Santhana V, Fidler TP, Sebag SC, Rasmussen TP, Mittauer DJ, Strack S, Goswami PC, Abel ED, et al. Loss of MCU prevents mitochondrial fusion in G1-S phase and blocks cell cycle progression and proliferation. *Sci Signal*. 2019;12. doi: 10.1126/scisignal.aav1439
25. Mitra K, Wunder C, Roysam B, Lin G, Lippincott-Schwartz J. A hyperfused mitochondrial state achieved at G1-S regulates cyclin E buildup and entry into S phase. *Proc Natl Acad Sci U S A*. 2009;106:11960-11965. doi: 10.1073/pnas.0904875106
26. Montemurro C, Vadrevu S, Gurlo T, Butler AE, Vongbunyong KE, Petcherski A, Shirihai OS, Satin LS, Braas D, Butler PC, et al. Cell cycle-related metabolism and mitochondrial dynamics in a replication-competent pancreatic beta-cell line. *Cell Cycle*. 2017;16:2086-2099. doi: 10.1080/15384101.2017.1361069
27. Birsa N, Norkett R, Higgs N, Lopez-Domenech G, Kittler JT. Mitochondrial trafficking in neurons and the role of the Miro family of GTPase proteins. *Biochem Soc Trans*. 2013;41:1525-1531. doi: 10.1042/BST20130234
28. Chang KT, Niescier RF, Min KT. Mitochondrial matrix Ca2+ as an intrinsic signal regulating mitochondrial motility in axons. *Proc Natl Acad Sci U S A*. 2011;108:15456-15461. doi: 10.1073/pnas.1106862108
29. Schwarz L, Sharma K, Dodi LD, Rieder LS, Fallier-Becker P, Casadei N, Fitzgerald JC. Miro1 R272Q disrupts mitochondrial calcium handling and neurotransmitter uptake in dopaminergic neurons. *Front Mol Neurosci*. 2022;15:966209. doi: 10.3389/fnmol.2022.966209

30. Niescier RF, Hong K, Park D, Min KT. MCU Interacts with Miro1 to Modulate Mitochondrial Functions in Neurons. *J Neurosci*. 2018;38:4666-4677. doi: 10.1523/JNEUROSCI.0504-18.2018
31. Castro IG, Richards DM, Metz J, Costello JL, Passmore JB, Schrader TA, Gouveia A, Ribeiro D, Schrader M. A role for Mitochondrial Rho GTPase 1 (MIRO1) in motility and membrane dynamics of peroxisomes. *Traffic*. 2018;19:229-242. doi: 10.1111/tra.12549
32. Kanfer G, Courtheoux T, Peterka M, Meier S, Soste M, Melnik A, Reis K, Aspenstrom P, Peter M, Picotti P, et al. Mitotic redistribution of the mitochondrial network by Miro and Cenp-F. *Nat Commun*. 2015;6:8015. doi: 10.1038/ncomms9015
33. Perez J, Hill BG, Benavides GA, Dranka BP, Darley-Usmar VM. Role of cellular bioenergetics in smooth muscle cell proliferation induced by platelet-derived growth factor. *Biochem J*. 2010;428:255-267. doi: 10.1042/BJ20100090
34. Zhang CY, Hu YC, Zhang Y, Ma WD, Song YF, Quan XH, Guo X, Wang CX. Glutamine switches vascular smooth muscle cells to synthetic phenotype through inhibiting miR-143 expression and upregulating THY1 expression. *Life Sci*. 2021:119365. doi: 10.1016/j.lfs.2021.119365
35. Park HY, Kim MJ, Lee S, Jin J, Kim JG, Choi YK, Park KG. Inhibitory Effect of a Glutamine Antagonist on Proliferation and Migration of VSMCs via Simultaneous Attenuation of Glycolysis and Oxidative Phosphorylation. *Int J Mol Sci*. 2021;22. doi: 10.3390/ijms22115602
36. Alshaabi H, Shannon N, Gravelle R, Milczarek S, Messier T, Cunniff B. Miro1-mediated mitochondrial positioning supports subcellular redox status. *Redox Biol*. 2021;38:101818. doi: 10.1016/j.redox.2020.101818
37. Alshaabi H, Heininger M, Cunniff B. Dynamic regulation of subcellular mitochondrial position for localized metabolite levels. *J Biochem*. 2020;167:109-117. doi: 10.1093/jb/mvz058
38. Moller A, Bauer CS, Cohen RN, Webster CP, De Vos KJ. Amyotrophic lateral sclerosis-associated mutant SOD1 inhibits anterograde axonal transport of mitochondria by reducing Miro1 levels. *Hum Mol Genet*. 2017;26:4668-4679. doi: 10.1093/hmg/ddx348
39. Nguyen TT, Oh SS, Weaver D, Lewandowska A, Maxfield D, Schuler MH, Smith NK, Macfarlane J, Saunders G, Palmer CA, et al. Loss of Miro1-directed mitochondrial movement results in a novel murine model for neuron disease. *Proc Natl Acad Sci U S A*. 2014;111:E3631-3640. doi: 10.1073/pnas.1402449111
40. Macaskill AF, Rinholm JE, Twelvetrees AE, Arancibia-Carcamo IL, Muir J, Fransson A, Aspenstrom P, Attwell D, Kittler JT. Miro1 is a calcium sensor for glutamate receptor-dependent localization of mitochondria at synapses. *Neuron*. 2009;61:541-555. doi: 10.1016/j.neuron.2009.01.030
41. Finkel T, Hwang PM. The Krebs cycle meets the cell cycle: mitochondria and the G1-S transition. *Proc Natl Acad Sci U S A*. 2009;106:11825-11826. doi: 10.1073/pnas.0906430106
42. Stephen TL, Higgs NF, Sheehan DF, Al Awabdh S, Lopez-Domenech G, Arancibia-Carcamo IL, Kittler JT. Miro1 Regulates Activity-Driven Positioning of Mitochondria within Astrocytic Processes Apposed to Synapses to Regulate Intracellular Calcium Signaling. *J Neurosci*. 2015;35:15996-16011. doi: 10.1523/JNEUROSCI.2068-15.2015
43. Cao Y, Xu C, Ye J, He Q, Zhang X, Jia S, Qiao X, Zhang C, Liu R, Weng L, et al. Miro2 Regulates Inter-Mitochondrial Communication in the Heart and Protects Against TAC-Induced Cardiac Dysfunction. *Circ Res*. 2019;125:728-743. doi: 10.1161/CIRCRESAHA.119.315432

LEGENDS

Figure 1

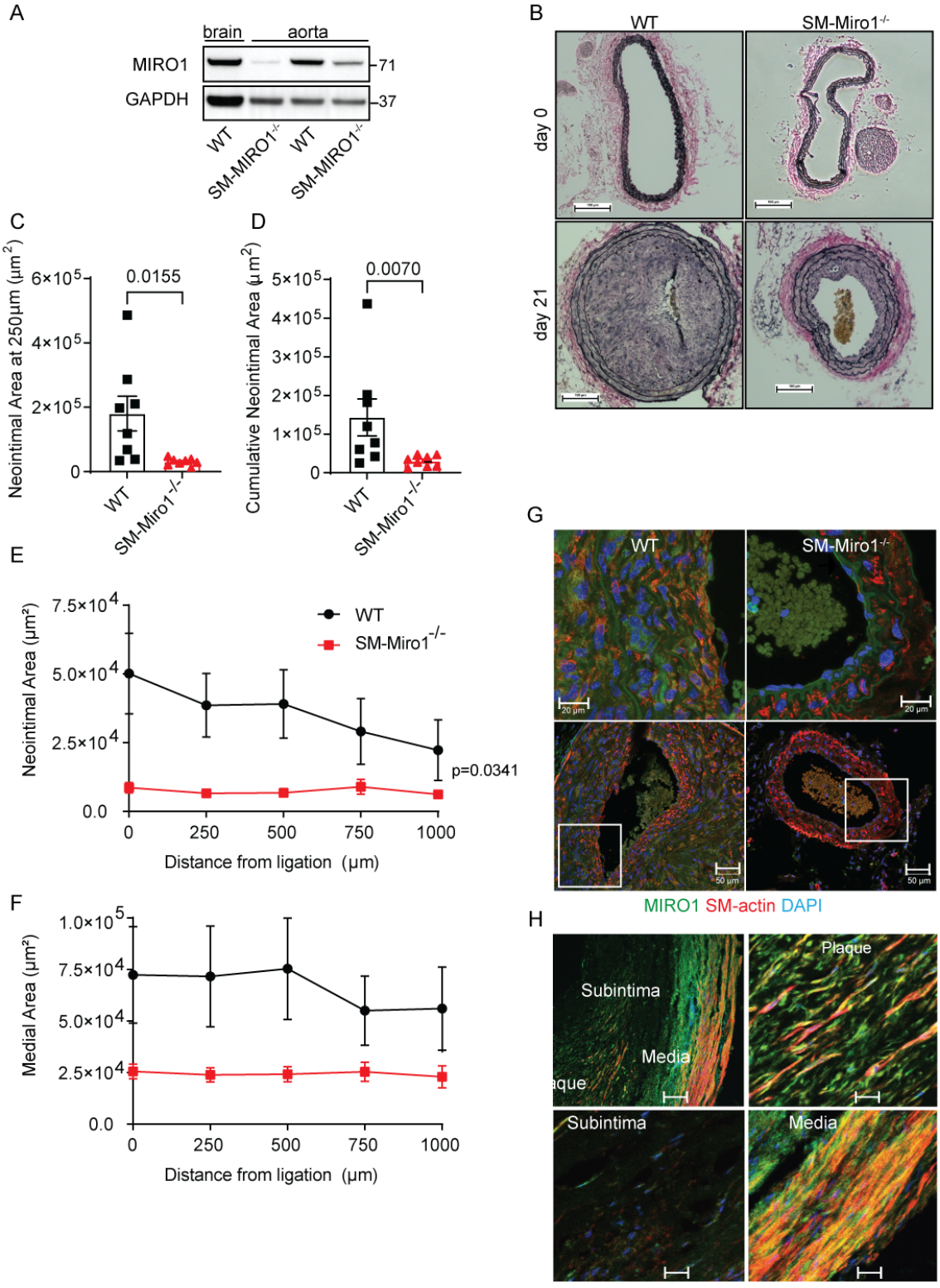

Figure 1. Loss of Miro1 blocks neointima formation.

(**A**) Immunoblots for MIRO1 in lysates from brain and aorta isolated from WT and SM-Miro1$^{-/-}$ mice.
(**B**) Verhoeff-Van Gieson staining in the unligated and ligated common carotid arteries of WT and SM-Miro1$^{-/-}$ mice, at 21 days post ligation. Scale bar = 100 µm.
(**C**) Neointimal area in ligated carotid arteries at 250 µm from the bifurcation (n=8). Neointimal area was determined by subtracting the luminal area from the area defined by the internal elastic lamina.
(**D**) Cumulative neointimal area, calculated from all neointimal areas within 1000 µm of the bifurcation.
(**E**) Neointimal area at the indicated distances from the site of ligation (n=8).
(**F**) Medial area at the indicated distances from the site of ligation (n=8). The medial area was determined by subtracting the area defined by the internal elastic lamina from the area defined by the external elastic lamina.
(**G**) Immunofluorescence of MIRO1 expression in the mouse carotid artery. MIRO1, green; SM-actin, red; DAPI, blue. Scale bar: 20 µm in upper images; 50 µm in lower images. Upper images are magnifications of the areas labeled with a box in the lower images.
(**H**) immunofluorescence of MIRO1 expression in a human coronary artery. MIRO1, green; SM-actin, red; DAPI, blue. Scale bar: 80 µm in left upper image; 20 µm right upper and both lower images).
Statistical analyses were performed using the Mann-Whitney test (C and D) or two-way ANOVA (E, F).

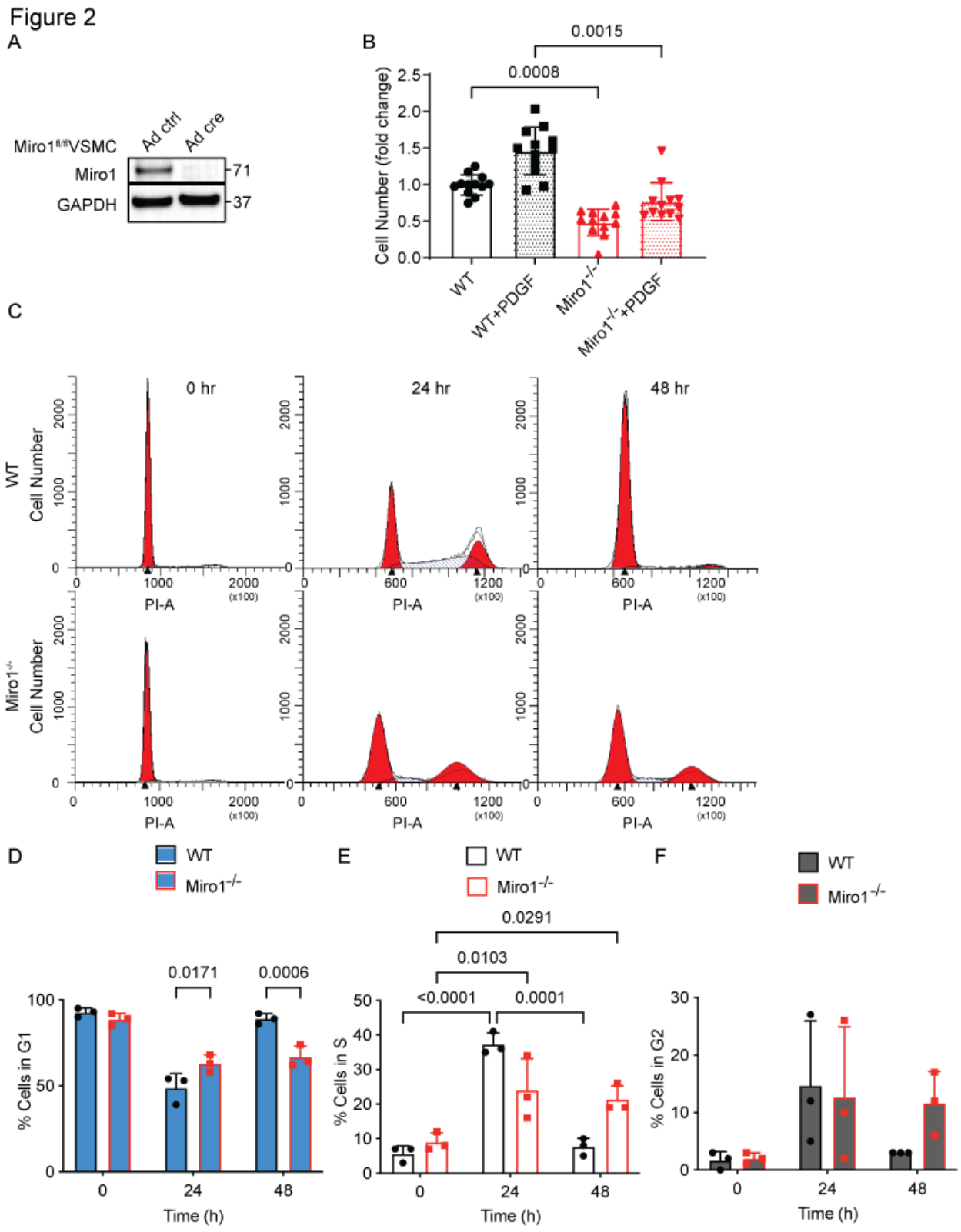

Figure 2. Loss of Miro1 reduces VSMC proliferation.

(**A**) MIRO1 levels in mitochondrial fractions of VSMCs from Miro1$^{fl/fl}$ mice transduced with adenovirus expressing Cre or control adenovirus, as determined by immunoblotting.

(**B**) Number of VSMCs from Miro1$^{fl/fl}$ mice following transduction with adenovirus expressing cre (MIRO1$^{-/-}$) or control (WT) adenovirus, at 72 hr after incubation with PDGF (20ng/ml) or control (saline), (n=12).
(**C**) DNA content of synchronized WT and MIRO1$^{-/-}$ VSMCs, as assessed by fluorescence-activated cell sorting (FACS). Times are 0, 24, and 48 hr after release from growth arrest for 48h in FBS-free media, and then at 24 and 48hr after release from arrest with media containing 10% FBS.
(**D-F**) Quantification of cell-cycle phase distribution of WT and MIRO1$^{-/-}$ VSMCs shown in C, (n=3).
Statistical analyses were performed using the Kruskal-Wallis test (B) and two-way ANOVA (D-F).

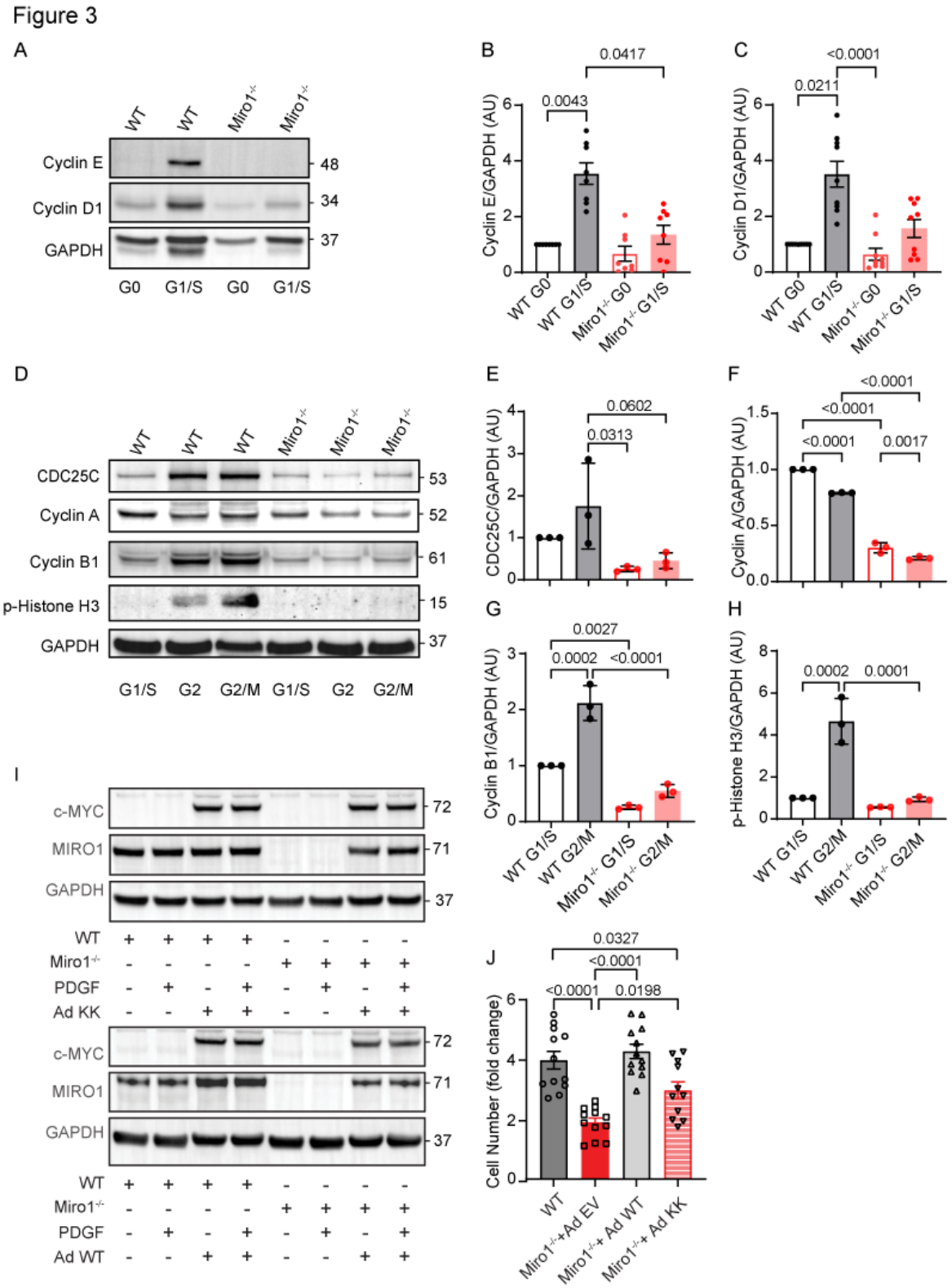

Figure 3. Loss of Miro1 reduces expression of cell cycle markers for G1/S and G/M cell cycle transition.

(**A**) Immunoblots for cyclin E and D1 as markers of the indicated cell cycle phases in whole-cell lysates of WT and Miro1$^{-/-}$ VSMCs following synchronization by serum starvation, at G0 (after

growth arrest for 48h in FBS-free media,), and G1/S (after release from growth arrest with media containing 10% FBS for 24 h.
(**B, C**) Quantification of Cyclin E and D1 levels on immunoblots like those shown in panel A (n=8).
(**D**) Levels of CDC25C, cyclins A, B1 and phosphorylated histone H-3 as markers of the G2 and M cell-cycle phases in whole-cell lysates of WT and Miro1$^{-/-}$ VSMCs following synchronization in G1/S phase by treatment with aphidicolin (5 µM for 24h), and then incubation in medium containing 10% FCS for 8 hr (G2) or 18 hr (G2/M).
(**E-H**) Quantification of protein levels from immunoblots as shown in D (n=3).
(**I**) Immunoblots for MIRO1 and c-MYC in WT and Miro1$^{-/-}$ VSMCs transduced with adenovirus expressing MIRO1-WT and MIRO1-KK.
(**J**) Number of WT and Miro1 $^{-/-}$ VSMCs transduced with adenovirus expressing MIRO1-WT, MIRO1-KK, or control adenovirus (empty vector, Ad EV) and treated with PDGF (20 ng/ml) for 72 hr (n=11).
Statistical analyses were performed by one-way ANOVA (B, C, E-H, J).

Figure 4

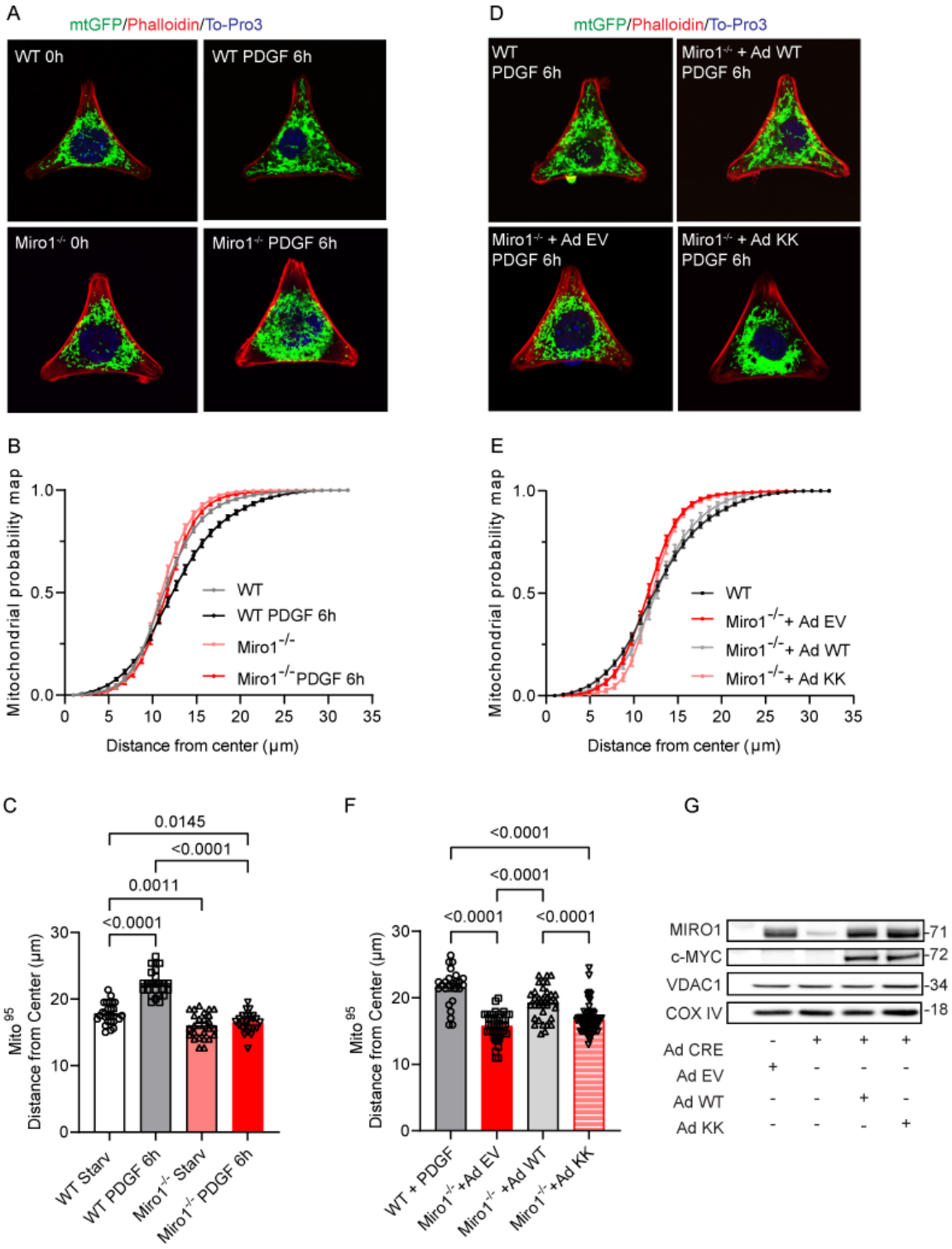

Figure 4. Loss of MIRO1 impairs mitochondrial mobility in proliferating VSMCs.

(**A**) Representative confocal images of WT and Miro1$^{-/-}$ VSMCs grown on Y-shaped adhesive micropatterns (CYTOOchips^{TM}), with VSMCs synchronized by serum starvation for 24 hr (0 hr

timepoint), followed by change to medium containing 10% FCS and PDGF (20ng/ml) for 6hr (Phalloidin, red; mitochondrial GFP, green; DAPI, blue).
(**B**) Mitochondrial probability map. The cumulative distribution of mitochondria was assessed for images as in (A) by modified Sholl's analysis. Data are plotted by growth conditions.
(**C**) $Mito^{95}$ values, defined as the distance from the center of the CYTOOchips^{TM} at which 95% of the mitochondrial signal is found, under the conditions used in (A).
(**D**) Representative confocal images of WT and $Miro1^{-/-}$ VSMCs grown on CYTOOchips^{TM}. $Miro1^{-/-}$ VSMCs were transduced with adenovirus expressing MIRO1-WT or MIRO1-KK for 72 hr before being seeded onto CYTOOchips^{TM}. The cell cycle was synchronized by serum starvation for 24 hr (not shown); the cells were subsequently treated with medium containing 10% FCS and PDGF (20ng/ml) for 6 hr.
(**E**) Mitochondrial probability map. The cumulative distribution of mitochondria was assessed for images shown in (D). Data are plotted as in B.
(**F**) $Mito^{95}$ values, as defined in (C) but under the conditions used in (D).
(**G**) Immunoblots for MIRO1 and c-myc in WT and $Miro1^{-/-}$ VSMCs transduced with adenoviruses expressing MIRO1-WT (Ad WT), MIRO1-KK (Ad KK), or with control adenovirus (empty vector; Ad EV).
Statistical analyses were performed by one-way ANOVA (C, F).

Figure 5

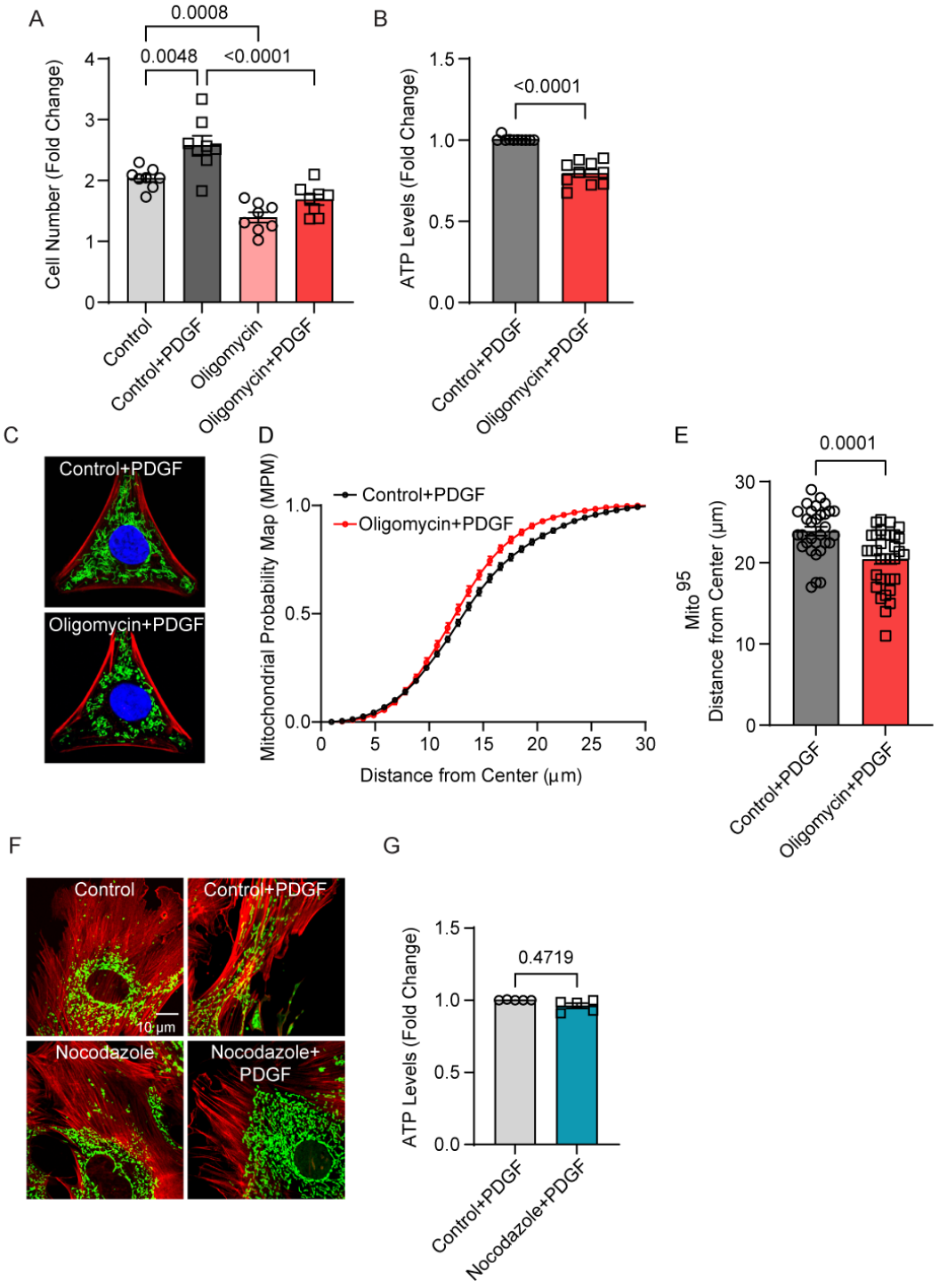

Figure 5. Inhibition of mitochondrial ATP production reduces VSMC proliferation, but inhibiting mitochondrial mobility does not affect ATP levels.

(**A**) Number of WT VSMCs after 72-hr treatment with either PDGF (20 ng/ml) and/or oligomycin (1 µM) (n=8).

(**B**) ATP levels in WT VSMCs after 16-hr treatment with PDGF (20 ng/ml) or with PDGF in addition to oligomycin (1 µM) (n=10).
(**C**) Representative confocal images of WT VSMCs on CYTOOchips^{TM} with Y-shaped micropatterns, following 16-hr treatment with PDGF (20 ng/ml) and oligomycin (1 µM). Mitochondria, green; phalloidin, red; DAPI, blue.
(**D**) Mitochondrial probability map. The cumulative distribution of mitochondria was assessed for images as in (C) by modified Sholl's analysis.
(**E**) Mito^{95} values, defined as the distance from the center of the Y-shaped pattern at which 95% of the mitochondrial signal is found for growing cells like in (C).
(**F**) Representative confocal images of WT VSMCs infected with mitoGFP and stained with phalloidin. Cells were synchronized by serum starvation for 48 hr and then released from starvation by replacing the medium with one containing 10% FBS and PDGF (20 ng/ml). Some samples were treated with nocodazole (1µM). Images were taken immediately after growth media (Control) or growth media with nocodazole was added (Nocodazole) and after incubation for 16 hr (Control + PDGF, Nocodazole + PDGF).
(**G**) ATP levels in WT VSMCs after 16-hr treatment in growth media with PDGF or growth media supplemented with PDGF and Nocodazole (1µM) (n=5).
Statistical analyses were performed by one-way ANOVA (A) or Mann-Whitney (B, E, G).

Figure 6

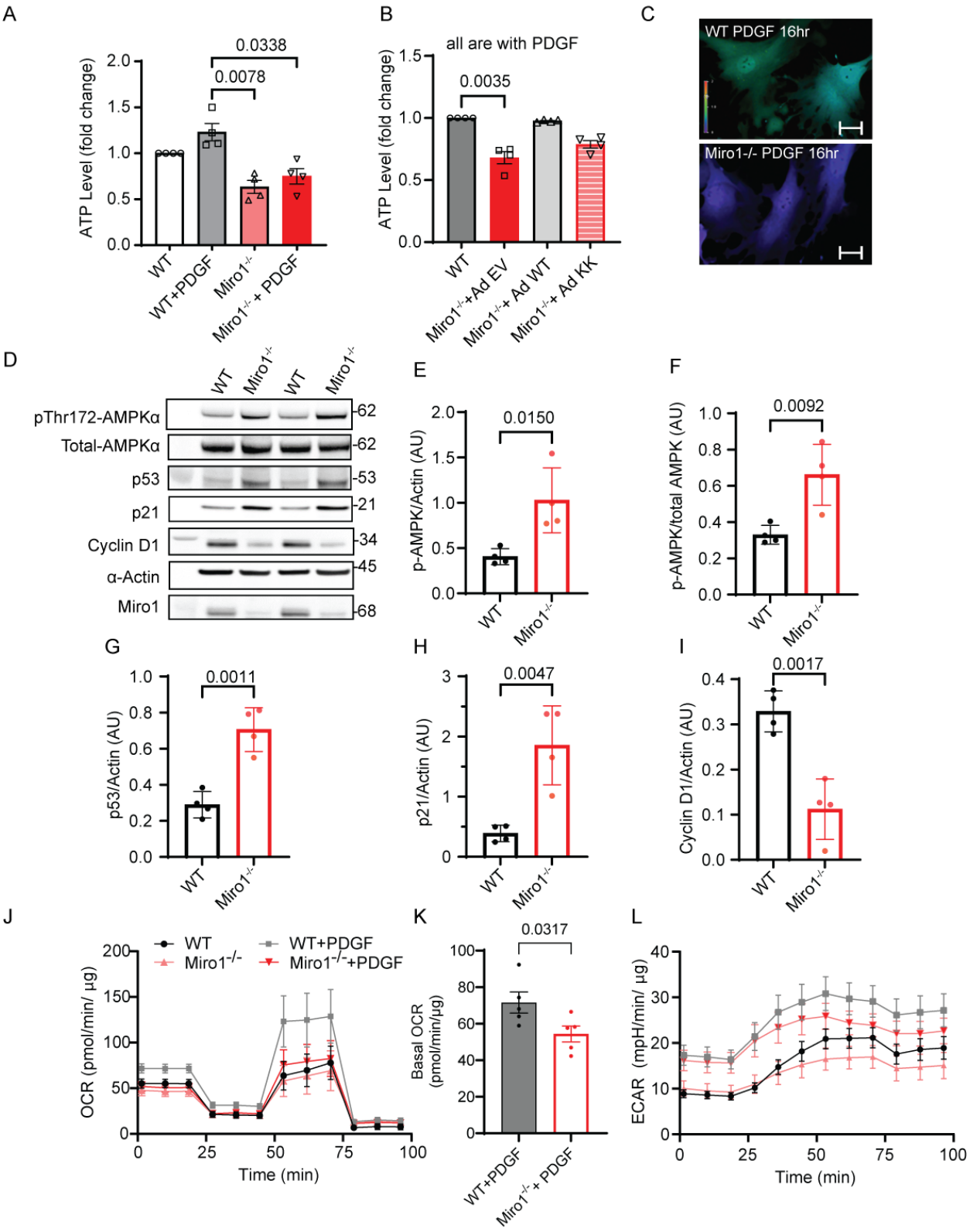

Figure 6. Loss of Miro1 leads to impaired mitochondrial metabolic activity and is associated with decreased proliferative capacity.

(**A**) Intracellular ATP levels in WT and Miro1$^{-/-}$ VSMCs after treatment with PDGF (20ng/ml for 16h) or control (no PDGF), normalized to levels in control WT VSMCs (no PDGF) (n=4).
(**B**) Intracellular ATP levels in WT and Miro1$^{-/-}$ VSMCs transduced with adenovirus expressing MIRO1-WT (Ad WT) or MIRO1-KK (Ad KK) or control adenovirus (empty vector, Ad-EV) after treatment with PDGF (20ng/ml for 16h) or control (no PDGF), normalized to ATP levels in control WT VSMCs (no PDGF)
(**C**) Representative images of WT and Miro1$^{-/-}$ VSMCs transduced with adenovirus expressing the fluorescent ATP sensitive protein pm-iATPSnFR1.0 after treatment with PDGF (20ng/ml for 16hr).
(**D**) Immunoblot of lysates from WT and Miro1$^{-/-}$ VSMCs for markers of the metabolic state (phosphorylated (p-Thr172) and total AMPKα), and cell cycle progression (p53, p21 and cyclin D1) at 48 hr after incubation in serum-free medium (cell-cycle arrest).
(**E-I**). Quantification of immunoblot signal in samples shown in (D) for (E) phosphorylated (p-Thr172) AMPKα normalized to actin, (**F**) phosphorylated (p-Thr172) AMPKα normalized to AMPKα, (G) p53, (H) p21, and (I) cyclin D1, all normalized to actin.
(**J**) Oxygen consumption rate (OCR), as determined by Seahorse, for WT and Miro1$^{-/-}$ VSMCs with and without PDGF treatment (20ng/ml for 16hr) (n=5).
(**K**) Quantification of basal OCR for WT and Miro1$^{-/-}$ VSMCs treated with PDGF (n=5).
(**L**) Extracellular acidification rate (ECAR), as determined by Seahorse, for WT and Miro1$^{-/-}$ VSMCs with and without PDGF treatment (20ng/ml for 16hr) (n=5).
Statistical analyses were performed by Kruskal-Wallis test (A, B), unpaired t-test (E-I), Mann-Whitney test (K).

Figure 7

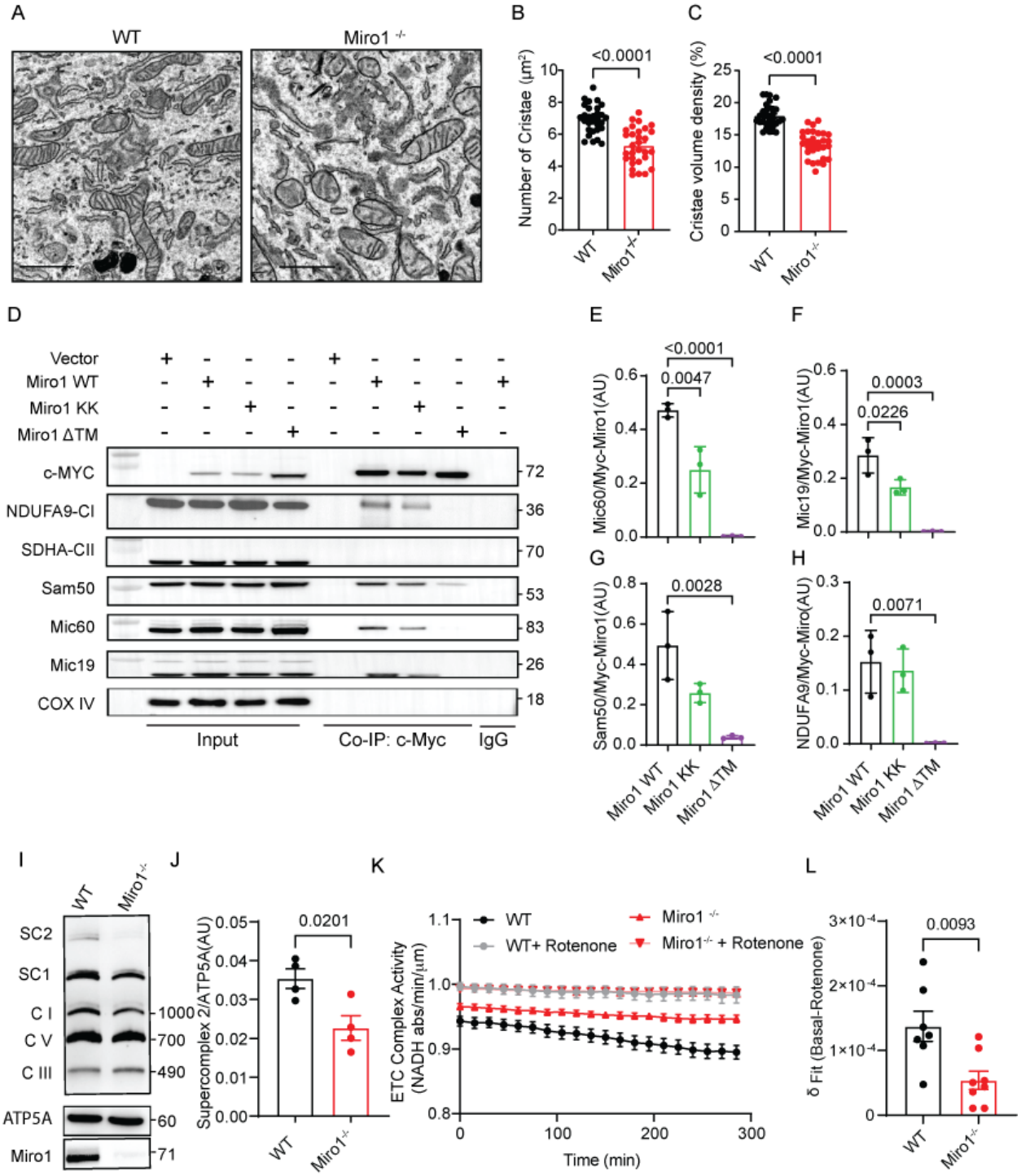

Figure 7. Loss of Miro1 leads to dysregulation of ETC activity under growth conditions.

(**A**) Representative transmission electron microscopy images of WT and Miro1$^{-/-}$ VSMCs.
(**B, C**) Quantification of (B) the number of mitochondrial cristae and (C) the volume density of the mitochondrial cristae in WT and Miro1$^{-/-}$ VSMCs.
(**D**) Levels of c-myc tagged MIRO1-WT, c-myc tagged MIRO1-KK, or MIRO1-ΔTM and proteins of the MIB/MICOS complex in HEK cells following pull-down assay, as determined by

immunoblotting. C-myc tagged Miro1 constructs were expressed in HEK cells for 72 hr before cell lysis and pull-down were performed.
(**E-H**) Quantification of (E) MIC60, (F) MIC19, (**G**) SAM 50, and (**H**) NDUFA9 in (D), adjusted for immunoprecipitated c-myc-tagged MIRO1 as in (**C**).
(**I**) Levels of mitochondrial supercomplex and ETC subunits in WT and Miro1$^{-/-}$ VSMCs, as determined by blue-native poly-acrylamide gel electrophoresis (BN-PAGE).
(**J**) Quantification of supercomplex 2 in (I) (n=4).
(**K**) Quantification of activity of ETC complex 1 in WT and Miro1$^{-/-}$ VSMCs, as determined by the decrease in the rate of absorbance at 340 nm with and without rotenone incubation for 10 min.
(**L**) Quantification of activity of ETC complex 1, plotted as the difference between absorbance curve slopes with and without rotenone (as in K) (n=7).
Statistical analyses were performed by Mann-Whitney (B, C, L), unpaired t-test (J), one-way ANOVA (E-H).